Author Manuscript

Author Manuscript

Author Manuscript

Author Manuscript

HHS Public Access

Author manuscript

Int J Dev Neurosci. Author manuscript; available in PMC 2017 February 01.

Published in final edited form as:

Int J Dev Neurosci. 2016 February ; 48: 58–70. doi:10.1016/j.ijdevneu.2015.11.007.

Endoplasmic Reticulum pathology and stress response in neurons precede programmed necrosis after neonatal hypoxia-ischemia

Raul Chavez-Valdez[a], **Debbie L. Flock**[a], **Lee J. Martin**[b], and **Frances J. Northington**[a]

Raul Chavez-Valdez: rchavez2@jhmi.edu; Debbie L. Flock: dflock1@jhmi.edu; Lee J. Martin: martinl@jhmi.edu; Frances J. Northington: frances@jhmi.edu

[a]Department of Pediatrics, Neonatal Research Laboratory, Johns Hopkins University School of Medicine. 600 N. Wolfe Street, CMSC 6-104. Baltimore, MD 21287, USA

[b]Departments of Pathology and Neuroscience, Johns Hopkins University School of Medicine. 720 Rutland Ave. Ross Research Building, Room 558. Baltimore, MD 21205, USA

Abstract

The endoplasmic reticulum (ER) is tasked, among many other functions, with preventing excitotoxicity from killing neurons following neonatal hypoxia-ischemia (HI). With the search for delayed therapies to treat neonatal HI, the study of delayed ER responses becomes relevant. We hypothesized that ER stress is a prominent feature of delayed neuronal death via programmed necrosis after neonatal HI. Since Necrostatin-1 (Nec-1), an inhibitor of programmed necrosis, provides delayed neuroprotection against neonatal HI in male mice, Nec-1 is an ideal tool to study delayed ER responses. C57B6 male mice were exposed to right carotid ligation followed by exposure to FiO_2=0.08 for 45 min at p7. Mice were treated with vehicle or Nec-1 (0.1 μl of 8 μmol) intracerebroventricularly with age-matched littermates as controls. Biochemistry assays at 3 and 24h and electron microscopy (EM) and immunohistochemistry at 96h after HI were performed. EM showed ER dilation and mitochondrial swelling as apparent early changes in neurons. With advanced neurodegeneration, large cytoplasmic fragments containing dilated ER "shed" into the surrounding neuropil and calreticulin immunoreactivity was lost concurrent with nuclear features suggestive of programmed necrosis. Nec-1 attenuated biochemical markers of ER stress after neonatal HI, including PERK and eIF2α phosphorylation, and unconventional XBP-1 splicing, consistent with the mitigation of later ER pathology. ER pathology may be an indicator of severity of neuronal injury and potential for recovery characterized by cytoplasmic shedding

CORRESPONDING AUTHORS: Drs. Raul Chavez-Valdez and Frances Northington. Department of Pediatrics Division of Neonatology, Johns Hopkins Hospital, 600 N. Wolfe Street, CMSC 6-104, Baltimore, MD 21287, USA. Telephone: (410) 955-4576; Fax: (410) 614-8388. rchavez2@jhmi.edu, frances@jhmi.edu.

ETHICS STATEMENT: We confirm that any aspect of the work covered in this manuscript involving experimental animals has been conducted with the ethical approval of all relevant bodies.

FINAL APPROVAL: All authors have approved the final version of this manuscript.

CONFLICT OF INTEREST: We confirm that there are no known conflicts of interest associated with this publication and there has been no significant financial support for this work that could have influenced its outcome.

Publisher's Disclaimer: This is a PDF file of an unedited manuscript that has been accepted for publication. As a service to our customers we are providing this early version of the manuscript. The manuscript will undergo copyediting, typesetting, and review of the resulting proof before it is published in its final citable form. Please note that during the production process errors may be discovered which could affect the content, and all legal disclaimers that apply to the journal pertain.

Author Manuscript Author Manuscript Author Manuscript Author Manuscript

distinct from apoptotic blebbing, that we term neuronal macrozeiosis. Therapies to attenuate ER stress applied at delayed stages may rescue stressed neurons after neonatal HI.

Keywords

Endoplasmic Reticulum Stress; Programmed Necrosis; Unfolded Protein Response; Neonatal Hypoxia-Ischemia; Cell Death; Cytoplasmic Shedding; Macrozeiosis

1. INTRODUCTION

Aberrant Ca^{2+} regulation and oxidative damage (Ferriero, 2004; Puka-Sundvall et al., 2000) are central to the basic biology of brain injury following neonatal hypoxia-ischemia (HI). The endoplasmic reticulum (ER) is tasked with preventing these insults from killing neurons (Paschen) *in vivo* and in cell culture. The ER responds to HI with morphologic and biochemical changes designed to contain and block propagation of these deleterious events. Initiation of the unfolded protein response (UPR) in response to neonatal HI is documented (Badiola et al., 2011; Carloni et al., 2014a) and UPR mitigation is associated with neuroprotection in multiple neonatal brain injury models with a variety of therapies (Carloni et al., 2014a; Carloni et al., 2014b; Zhu et al., 2014).

Studies of ER stress in neurodegenerative conditions suggests a role in failed neuroprotection or neuronal maintenance on a more chronic basis (Paschen and Mengesdorf). ER stress and autophagy pathways can cooperate as well (Sheng et al., 2012). Morphologic changes in ER structure are linked to stimuli known to cause neurodegeneration. Enlargement of the intraluminal ER capacity is considered a survival mechanism designed to allow more time for handling of misfolded proteins in culture (Bernales et al., 2006) and greater sequestration of Ca^{2+}. ER stress signaling is acutely activated in models of neonatal brain injury. Rough ER containing intraluminal Ca^{2+} precipitates are present in immature rat brain after HI (Puka-Sundvall et al., 2000); however, no investigation into ER stress beyond the acute injury period in neonatal brain injury has been undertaken.

We have shown that a delayed phase of neurodegeneration is a major component of neonatal brain injury after HI (Northington et al., 2001). Hence, we hypothesized that ER stress is a prominent feature of this delayed neuronal injury and that it may be part of the programmed necrosis form of neurodegeneration that we have described associated with neonatal HI (Chavez-Valdez et al., 2012a; Chavez-Valdez et al., 2012b; Northington et al., 2011). Importantly, necrostatin-1 (Nec-1), an allosteric inhibitor of receptor interacting protein kinase 1, blocks mitochondrial failure and oxidative injury to proteins during the acute phase after neonatal HI in mouse (Chavez-Valdez et al., 2012a; Northington et al., 2011); yet, its neuroprotective effect is not evident until 96 hours after injury (Northington et al., 2011). With the search for therapies to apply beyond the acute phase of injury, investigation of delayed ER stress is highly pertinent in neonatal brain injury research and Nec-1 is an ideal therapeutic tool to that end. In this study we sought to determine i) whether ER stress in neurons has a prominent presence after the acute phase of injury as witnessed by ultrastructural assessment, ii) how ultrastructural pathology may relate to the progression

Author Manuscript Author Manuscript Author Manuscript Author Manuscript

toward neurodegeneration, and iii) the efficacy of Nec-1 to mitigate early biochemical indicators of ER stress and delayed ER pathology.

2. METHODS AND METHODS

2.1 Animals

Neonatal male mice were used. Experiments were performed with approval by the Institutional Animal Care and Use Committee at Johns Hopkins University School of Medicine and they were carried out in accordance with the National Institute of Health Guide for the Care and Use of Laboratory Animals (8^{th} edition, NIH Publications) revised in 2011 and EU Directive 2010/63/EU for animal experiments. A total of 72 male mice were used for experiments. All efforts were made to minimize the number of mice used and their suffering. Male mice were chosen for the present study because in our hands, they sustain a more consistent injury after HI and have demonstrated a more consistent therapeutic response to treatment with Nec-1 at the same dose used for the current experiments (Northington et al., 2011).

2.2 Rice-Vannucci Model of Neonatal HI brain injury

HI was induced in male C57B6 mice at postnatal day (p) 7 using a modification of the Rice-Vannucci procedure for mice (Ditelberg et al., 1996). Mice were exposed to a second brief period of anesthesia with isofluorane followed by an intracerebroventricular (ICV) injection of 0.1 μl of 8 μmol Nec-1 (Calbiochem-EMD Chemicals Group, Gibbstown, NJ), or vehicle, methyl-β-cyclodextrin (Sigma, St Louis, MO, USA) 15 min after the end of 45 min of hypoxic exposure (FiO_2 =0.08). The dose of Nec-1 used for the current set of experiments has been proven to attenuate early biochemical changes and prevent delayed histological injury in forebrain of neonatal male mice exposed to experimental HI (Chavez-Valdez et al., 2012a; Northington et al., 2011). Pups were killed at 3h and 24h after HI (n = 6–8 pups/time/treatment) for biochemical analysis. Naive controls were age-matched littermates not exposed to HI or treatments. Mice were killed with an exposure to 20% (v/v) mixture of isoflurane in propylene glycol via one drop exposure method (Markovic and Murasko, 1993) and then decapitated. Brain was micro-dissected separating the hemispheres at the level of longitudinal cerebral fissure, removing the cerebellum at the level of transverse fissure, and isolating tissue above and lateral to the fornix to include hippocampus, striatum and cortex (forebrain) as previously described (Chavez-Valdez et al., 2014). Tissues were rapidly frozen (−80°C) for protein and qRT-PCR analysis (n= 4 pups/treatment/time/experiment). A separate group of mice were used for electron microscopy and immunohistochemistry as described in section 2.3.

2.3 Electron Microscopy (EM) and Immunohistochemistry (IHC) Tissue preparation

For EM and IHC, animals were killed with an overdose of isoflurane as above, and exsanguinated with cold 0.1 M PBS (pH7.4) via intra-cardiac perfusion (n=12, 4 pups/treatment). Brains were perfusion fixed with either 2% gluteraldehyde/2% paraformaldehyde for EM, or 4% paraformaldehyde/0.1M PBS for 30 min at 4 ml/min for IHC. Tissue was prepared for EM at the Cell Biology Imaging Facility, Johns Hopkins University. Briefly, tissue pieces from ipsilateral sensory motor cortex ($3mm^3$) were fixed in

Author Manuscript Author Manuscript Author Manuscript Author Manuscript

2% paraformaldehyde, 2% glutaraldehyde, 0.1 M sodium cacodylate, 3 mM CaCl2, at pH 7.4 overnight at 4 ºC. Following buffer rinse, samples were post-fixed in 1% osmium tetroxide, 0.1 M sodium cacodylate, 3 mM CaCl2 for 2 hr on ice in the dark. After a brief dH2O rinse, samples were incubated in 2 % uranyl acetate (0.22 um filtered) for 1 hour at room temperature, in the dark. Following en-bloc staining tissue samples were dehydrated through a graded series of ethanol to 100%, transferred through propylene oxide and embedded in Pelco Eponate 12 (Ted Pella. Inc. Redding, CA) and cured at 60 ºC for two days. Sections were cut on a Reichert Ultracut E with a 35^0 angle (compression free) Diatome Diamond knife. Thin sections (80 nm) were collected on formvar coated 1 × 2 mm copper slot grids and stained with uranyl acetate followed by lead citrate. Grids were viewed on a Hitachi 7600 TEM operating at 80 kV and digital images captured with an AMT XR-50 (5 megapixel) CCD camera.

For IHC tissues were cryoprotected with graded immersion in 15% and then 30% sucrose in PBS until the tissue sank, then frozen and stored at −80° C until cut at 50μm on a freezing microtome (Northington et al., 1996). Floating IHC for calreticulin was performed as previously described (Northington et al., 1996) with 1:500 dilution of whole rabbit antisera anti-calreticulin antibody (Novus Biologicals USA, Littleton, CO). Goat anti-rabbit antibody (1:200) was used as the secondary antibody and 3,3′-diaminobenzidine (DAB) as the chromagen (Northington et al., 1996). Tissues were counterstained with cresyl violet after developing in DAB.

Cortical neurons were assessed by EM and IHC to determine the intermediate stages of ER pathology in those injured neurons that survived neonatal HI at delayed stages. Morphological ER features in cortical neurons were most relevant to study given that forebrain tissue, which is mostly cortical tissue, was used for the biochemical assays. Because of the severity of hippocampal injury soon after neonatal HI and the smaller contribution of hippocampus in the forebrain homogenates, hippocampal neurons were considered less well suited for evaluating delayed ER pathology and cell death.

2.4 Gene expression by real time qRT-PCR

Total RNA was extracted from forebrain harvested from mice exposed to neonatal HI and treatments as described above (n=4 pups/treatment/time). PureLink™ RNA mini kit purification system (Invitrogen, Carlsbad, CA) was used according to manufacturer specifications. Approximately 1μg of total RNA was used for generation of complementary DNA (cDNA) using iScript cDNA synthesis kit (BioRad, Hercules, CA). Reverse transcription protocol included 5 min at 25°C; 30 min at 42°C and 5 min at 85°C. cDNA was then used to amplify target gene by real time qRT-PCR using 300 nM concentration of specific primers (Table 1). The amplification protocol included 40 cycles of 30 sec at 95.0 °C, 60 sec at 61 °C and 60 sec at 72.0 °C. GADPH (forward: 5′-TTGTCAAGCTCATTTCCTGGTATG-3′; reverse: 5′-GCCATGTAGGCCATGAGGTC-3′; 76-bp PCR product) and β-actin (forward: 5′-CCCAACTTGATGTATGAAGG-3′; reverse: 5′-TTGTGTAAGGTAAGGTGTGC-3′; 119-bp PCR product) were evaluated as housekeeping genes using the BestKeeper approach to determine stability of gene expression under experimental conditions (Pfaffl et al., 2004) as previously reported

Author Manuscript Author Manuscript Author Manuscript Author Manuscript

(Chavez-Valdez et al., 2012a). Based on its mRNA stability, β-actin expression was used as the denominator for calculations. Fold difference in gene expression was corrected to β-actin using the Pfaffl method (Pfaffl, 2001). Except for XBP-1, melting curves confirmed amplification of single PCR products. Multiple XBP-1 PCR products are shown by 1.3% agarose gel electrophoresis. Results were reported as fold change in gene expression relative to expression in age-matched naive control mice.

2.5 Protein levels

Mouse forebrain homogenates were prepared in homogenization buffer with phosphatase and protease inhibitors and 20% (w/v) glycerol (n=4 pups/treatment/time). Final concentrations of protein were determined using the Bradford assay (Bradford, 1976). Aliquots of forebrain homogenate (25 μg of total protein) were diluted 3:1 (v:v) in 4X loading buffer under reducing conditions and loaded into 4–30% pre-casted polyacrylamide gels (Bio-Rad Lab Inc, Hercules, CA). Protein was transferred to nitrocellulose membrane using the Trans-Blot Turbo Transfer System® (Bio-Rad Lab Inc, Hercules, CA), stained with Ponceau S, blocked with 2.5% nonfat dry milk with 0.1% Tween-20 in 50 mM Tris buffered saline (TBST, 50mM Tris/HCl and 150 mM NaCl, pH 7.4) except for pPERK, PERK, and eIF2α antibodies, which were blocked in 2.5% BSA. Nitrocellulose blots were incubated overnight at 4°C with primary antibodies. Positive controls were used to ascertain identification of target protein (see details below in section 2.6). After exposure to each primary antibody, membranes were washed with TBST, exposed to secondary antibodies for 1h and then developed with enhanced chemiluminescence using Clarity Western ECL Substrate (Bio-Rad, Hercules, CA). To quantify protein immunoreactivity, films were scanned using Adobe Photoshop (Adobe Systems Inc., San Jose, CA), and optical density (OD) was determined with NIH Image J Software (NIH, Bethesda, MD) adjusted for background. The reliability of sample loading and protein transfer was verified by immunoblotting nitrocellulose membranes for β-actin.

2.6 Positive controls and antibodies

Positive controls. PERK: 25 μg of NIH-3T3 cell lysate (sc-2210, Santa Cruz Biotechnology). GRP78, and fodrin αII: 10 μg of human cervical carcinoma lysate (HeLa cells, BD-611450, Becton Dickinson Biosciences). *Antibodies.* Anti-GRP78 (sc-13968, Santa Cruz Biotechnologies): rabbit polyclonal IgG raised against epitope corresponding to amino acids 525–653 mapping at the C-terminus of GRP78 of human origin and detecting a band at 78 kDa (0.5 μg/mL). Anti-PERK (CS-3192, Cell Signaling Technologies): rabbit monoclonal IgG raised against a synthetic peptide corresponding to the sequence of human PERK and detecting a band at 140 kDa (2 μg/mL). Anti-phosphorylated (Thr981) PERK (sc-32577, Santa Cruz Biotechnologies): rabbit polyclonal raised against a short amino acid sequence containing Thr981 phosphorylated PERK of human origin and detects a band at 140 kDa (0.5 μg/mL). Anti-eIF2α (cs-2103, Cell Signaling Technologies): mouse monoclonal raised against purified recombinant eIF2α and detecting a single band at 38 kDa (1 μg/mL). Anti-phosphorylated (Ser51) eIF2α (CS-3398, Cell Signaling Tech.): rabbit monoclonal against a synthetic phospho-peptide corresponding to residues surrounding Ser51 of human origin and detecting a band at 38kDa (1 μg/mL). Anti-GADD34 (sc-8327, Santa Cruz): rabbit polyclonal IgG raised against an epitope corresponding to amino acids

Author Manuscript Author Manuscript Author Manuscript Author Manuscript

483–674 of GADD34 of human origin and detecting a band at 73 kDa (1 μg/mL). Anti-CHOP (cs-5554, Cell Signaling Technologies): rabbit monoclonal IgG raised against a synthetic peptide corresponding to residues surrounding Leu159 of human CHOP protein and detecting a band at 27 kDa (2 μg/mL).

2.7 Statistics

Analysis of variance (ANOVA) was used with post-hoc pair analysis using Tukey's test for analysis of multiple normally distributed groups when analyzing protein data. The results were reported as mean ± SEM and represented as bar graphs. Gene expression data were not normally distributed, thus Mann-Whitney U test was used for analysis. Fold-changes in gene expression relative to age-matched naive control were represented as box and whisker plots, where the boxes were limited by the 25th and 75th percentiles and the solid line within the box represented the median. Significance was assigned to a p value ≤ 0.05 in all cases. Analysis was performed using IBM SPSS Statistics 18.0 software (IBM Corporation, Armonk, NY).

3. RESULTS

3.1 Marked ER pathology occurs in cortical neurons following neonatal HI

EM was used to assess the ultrastructural pathology in neurons of cerebral cortex of mice at 4 days after neonatal HI at p7. Cortical samples from mice without frank infarcts were studied, allowing for the characterization of organelle pathology in individual selectively vulnerable neurons. The degeneration of neurons in cerebral cortex was asynchronous permitting the reconstruction of an apparent evolution of neurodegeneration that was representative in several mice (Figs. 1, 2). Neurons at early stages of degeneration were distinct from morphologically normal neurons in cerebral cortex because of their overall darkness resulting from heavy metal contrast-staining and because of their prominent ER within the cytoplasm (Figs. 1A–C, 2A). These cells were identified unequivocally as neurons because they were contacted by axosomatic synapses. In these cells, the ER was prominent because it appeared as numerous sharply delineated vermiform strands and, in many instances, was marginated to the periphery of the neuron (Fig. 1A–C). These neurons also had nuclear changes that appeared initially as an overall more darkly contrasted nucleoplasmic matrix (Fig. 1A) to a nuclear matrix with slight condensation appearing as dark speckles throughout the nucleus (Fig. 1B,C). The next major morphological event in degenerating cortical neurons was marked dilatation and swelling of the ER (Figs. 1D, E, 2B, C). The pathological progression from ER strands to dilatation was concluded based on the similar location within the cell and general contour of the dilated organelle (Fig. 1A–E). The ER pathology further advanced with the formation of large swollen cisterns that were still recognizable as ER (Figs. 1F, 2C). The ER cisterns became large enough to envelop portions of cytoplasm, sometimes including mitochondria (Figs. 1G–I, 2D). These large dilated cisterns were noted to be ER-derived because of their continuity with the nuclear envelop (Fig. 1G–H). The nuclear pathology in these neurons was not as evidently staged as the ER pathology. Some neurons at the stage of ER swelling (Fig. 1F) showed extensive dark speckle formation within the nucleus, while other neurons with large cisterns continuous with the nuclear envelop could be found with condensed nuclear speckles or

Author Manuscript Author Manuscript Author Manuscript Author Manuscript

condensed material along the nuclear envelop (Fig. 1G–H). At the later stages of this neurodegeneration, cells with large swollen mitochondria appeared to have lost cytoplasmic volume and were shrunken. In favorable micrographs, some neurons were found with large cytoplasmic fragments that appeared to be in the process of being shed (Fig. 1H). Close scrutiny of the neuropil of cerebral cortex with degenerating neuronal cell bodies, revealed fragments of cells containing ER cisterns with enveloped cytoplasm and swollen mitochondria clearly delineated by cell membrane (Fig. 2D,E). These shed fragments were easily distinguished from swollen dendrites (Fig. 2E) in the neuropil which appeared to have much less protein content and thus a lighter background and frequently contained swollen disrupted mitochondria but no ER. Microglia were often found in the area of neurons with marked ER pathology and shed cytoplasmic fragments (Fig. 2F).

Additional details of ER pathology in cortical neurons following neonatal HI were confirmed by immunostaining for calreticulin, an ER chaperone protein, and light microscopic assessments (Fig 2G–L). Baseline immunoreactivity for calreticulin in cortical pyramidal neurons in the developing brain was seen in the soma in a pattern consistent with distribution within the ER (Fig. 2G). Calreticulin was increasingly abundant in neurons in more injured areas of the cortex (Fig 2H–J); reaching a point in more injured areas where some neurons had prominent calreticulin immunoreactive globules filling the cytoplasm and nearby neurons had little staining in a pattern suggesting breakdown of the cell and shedding of ER fragments (Fig. 2K). In the most severely injured regions, sparse neuronal calreticulin was appreciated and large numbers of microglia were present (Fig. 2L).

3.2 HI-induced programmed necrosis involves early activation of ER stress UPR and ER pathology

To determine a possible role for ER pathology in programmed necrosis induced by neonatal HI, we first assayed for the cleaved products of αII-fodrin in forebrain to confirm biochemical injury and protection with Nec-1. Calpain-dependent cleavage of αII-fodrin into 150 kDa products (Gill and Perez-Polo, 2009; Wang, 2000) was robust in mice at 3h and 24h following HI and was prevented by treatment with Nec-1 (Fig. 3A). At 3h after HI, vehicle-treated mice had 38% ($p=0.009$ vs. naive) and 33% ($p=0.01$ vs. Nec-1 treated) greater 150kDa: 240kDa αII-fodrin ratio (ANOVA, $p=0.006$; n=4/group). This effect persisted at 24h ($p=0.01$ vs. naive; ANOVA, p=002). Similarly, caspase-dependent cleavage of αII-fodrin into 120 kDa products (Wang, 2000) after HI was also increased at 3h (55% higher 120 kda : 240 kDa ratio, $p=0.002$ vs. naive.) in vehicle treated mice, and persisted by 24h after HI (Fig. 3B). Nec-1 delayed, but did not prevent the cleavage of αII-fodrin to its 120 kDa fragment (at 3h $p=0.05$ vs. vehicle, at 24h $p>0.05$ vs vehicle, 3h ANOVA, $p=0.003$; 24h ANOVA, $p=0.03$). To determine whether HI-induced ER ultrastructural changes were prevented by Nec-1, known to provide neuroprotection at 4 days (p11) following HI (Northington et al., 2011), we assessed ER morphology and biochemistry following HI and treatment with Nec-1 and vehicle. In neurons from vehicle-treated mice following neonatal HI, the full spectrum of ER pathology is found including moderate dilation (Fig. 4A) to very enlarged ER cisterns embracing cytoplasmic contents (Fig. 4B) to large dilations with complete separation from the nuclear membrane (Fig. 4C). This ER pathology occurred along with mitochondrial disruption and nuclear pathology ranging from minimal nuclear

Author Manuscript Author Manuscript Author Manuscript Author Manuscript

chromatin condensation through larger clumps to perimembrane chromatin clumping (Fig. 4A–C). Numerous apparently shed fragments of cytoplasm (Fig. 4D) were found in the neuropil in injured areas. These fragments contained massively dilated ER with cytoplasmic engulfment surrounded by a cell membrane. In contrast, only minimal ER pathology was seen in the mice treated with Nec-1 following HI (Fig. 4E–H). No ER, mitochondrial or nuclear pathology was evident despite mild disruption of the neuropil (Fig. 4E). Minimal dilation of rare segments of ER occurred with some darkened mitochondria (Fig. 4F). Early stage dilation in elongated segments of ER in conjunction with very minor chromatin clumping was the most advanced from of ER pathology in Nec-1-treated mice (Fig. 4G) despite the presence of neuropil disruption. Overall the neuropil was free from apparently-shed cytoplasmic fragments but did contain occasional swollen and disrupted dendritic profiles (Fig. 4H).

3.3 Phosphorylation of ER sensors, PERK, and IRE1 are fundamental markers of activation of the UPR in forebrain after neonatal HI

To determine whether ultrastructural features of prominent ER pathology followed earlier activation of the UPR, and whether changes in the UPR were influenced by treatment with Nec-1, we examined ER protein quality control signaling cascades at 3 and 24 hours following HI in mice treated with vehicle or Nec-1. GRP78, is a master ER stress regulator (Moreno and Tiffany-Castiglioni, 2015) binding to ER sensors at baseline and changing its binding partners in the face of stress. Neither HI nor Nec-1 treatment had an effect on GRP78 mRNA and protein levels at 3 or 24 hours after HI (Fig. 5A–B, n=6 per group). By western blotting PERK phosphorylation was found to be increased in vehicle-treated mice following HI (53%, 3h after HI, p=0.04 vs. naive control, Fig. 5C) and this increase was delayed by treatment with Nec-1 (ANOVA, p=0.04; n=4/group). At 24 h after HI, there was a similar increase in PERK phosphorylation in Nec-1 treated mice (68%, p=0.02 vs. naive; ANOVA, p=0.01, Fig 5C). An increase in eIF2α phosphorylation coincided with PERK phosphorylation in vehicle-treated mice at 3h after HI (108%, p=0.01 vs. naive, n=4 per group, Fig 5D). This second step in UPR activation did not occur in Nec-1 treated mice at 3 or 24h after HI.

During ER stress, XBP-1 mRNA expression increases downstream of eIF2α phosphorylation (Yoshida et al., 2000) and XBP-1 mRNA undergoes unconventional splicing (Calfon et al., 2002; Yoshida et al., 2001). Vehicle-treated mice demonstrated a robust and sustained increase in XBP-1 transcription from 3–24h following HI by 3.8-fold (p=0.02) and 4.7-fold (p=0.01 vs. naive), respectively (Fig 5E). Nec-1 attenuated the XBP-1 mRNA increase at 3h (p=0.03 vs. naive) and completely blocked the HI induced increase at 24h. Electrophoresis of PCR products showed processed XBP-1(s) transcripts below 600-bp most prominently in a vehicle treated mouse at 3h and 24h after HI (Fig 5F).

Downstream events meant to provide feedback to the UPR were altered in response to neonatal HI and Nec-1 treatment. In concert with the increase in PERK and eIF2α phosphorylation at 3h, GADD34 mRNA expression increased 4.5-fold in vehicle-treated mice at 3h (p=0.02 vs. naive, n =6/group (Fig. 5G). By 24h the increase in GADD34 mRNA in vehicle-treated mice abated. Again Nec-1 treated mice had a delayed response in this

Author Manuscript Author Manuscript Author Manuscript Author Manuscript

stage of the UPR with a 2-fold increase in GADD 34 mRNA delayed to 24h (p =0.04 vs. naive) in concert with the delayed pPERK response (Fig. 5G). Despite these mRNA changes, only the mRNA response in vehicle-treated mice translated to a change in GADD34 protein with a 117% increase (p=0.04 vs. naive; ANOVA, p=0.04; n = 6/group; Fig. 5H).

Expression of CHOP in response to an overwhelming ER stress is considered a final arbiter of cell death (Szegezdi et al., 2006). In the present model, CHOP gene expression was up-regulated by ~2.3-fold (p=0.01) and 4.5-fold (p=0.02 vs. naive control) at 3h and 24h after HI (Fig. 5I). This response was not modulated by treatment with Nec-1. A modest (~20%, p<0.05 vs. naive control) increase in CHOP protein levels was seen at 24h after HI with no effect on this response by Nec-1 treatment. (ANOVA, p=0.05; n=6/group, Fig 5J).

4. DISCUSSION

This study reveals several new findings relevant to the mechanisms of neurodegeneration after HI in neonatal mice. ER stress is initiated quickly after HI, continues for a prolonged period, and when unabated is associated with major intracellular pathology that drives a form of programmed necrosis (Fig 6), that can be attenuated by Nec-1. These novel findings of ER ultrastructural pathology following initial stimulation of the UPR fit well conceptually with the idea that neonatal brain injury is initiated early, and has prolonged and ongoing pathologic mechanisms that, if left unabated result in further injury to the neonatal brain (Ferriero, 2004), but may be modified by drug therapy implemented after the initial phase of acute energy failure. The ER functions include intracellular Ca^{2+} homeostasis and protein synthesis, post-translational modification, and folding. As a result of ER stress UPR is activated. While short lasting activation of UPR is a mechanism of compensation by globally inhibiting protein synthesis preventing further accumulation of unfolded proteins within the ER, sustained activation of the PERK/eIF2α UPR signaling has been associated to neurodegeneration linked to tauopathies such as Alzheimer's disease and dementia (Hoozemans et al., 2005; Radford et al., 2015). ER stress has been recognized in all major forms of neurodegeneration including Parkinson's disease, Alzheimer's disease, Huntington's disease, amyotrophic lateral sclerosis, as well as HI and excitotoxicity (Paschen; Placido et al., 2015). Compared to the mature brain, the neonatal brain may be particularly vulnerable to ER stress following HI injury, perhaps secondary to deficient upregulation of the chaperone protein GRP78 as reported here and by others (Sun et al., 2015). The mechanistic role of ER stress in the evolution of neonatal HI injury is further documented by the neuroprotective effects of ICV dantrolene, a ryanodine receptor antagonist, in rats (Gwak et al., 2008; Tasker et al., 1998). The importance of ER stress in neonatal brain injury is also highlighted by the utility, as a biomarker, of Ubiquitin Carboxyl-Terminal Hydrolase Isozyme L1 (UCH-L1), a neuron-specific protein that allows misfolded proteins to be targeted to the proteasome (Chalak et al., 2014; Douglas-Escobar et al., 2010; Massaro et al., 2013). As would be expected, several treatments known to provide neuroprotection against neonatal HI attenuate ER stress as a mechanism of their therapeutic effect. ER stress is decreased by ischemic pre-conditioning (Sheng et al., 2012), ischemic post-conditioning (Yuan et al., 2011), nNOS inhibition (Krishnamoorthy and Shyam, 2012), rapamycin, and melatonin (Carloni et al., 2014a; Carloni et al., 2014b).

Author Manuscript Author Manuscript Author Manuscript Author Manuscript

Early engagement of the UPR with phosphorylation of the stress sensor PERK and eIF2α, sustained increase in XBP-1 transcription, increase in CHOP mRNA and protein, and reciprocal increase of GADD 34, to provide negative feedback was consistent with activation of the UPR in both *in-vivo* and in cell culture models of neonatal brain injury (Badiola et al., 2011; Carloni et al., 2014a). The timing of up-regulation of various UPR components in our model accords with other work on UPR in neonatal HI and OGD (Badiola et al., 2011). They, too, found rapid and transient inhibition of protein synthesis after injury and robust signaling by GADD 34 for reversal of the protein synthesis inhibition within 24 hours after injury (Badiola et al., 2011). Given that Nec-1 robustly and persistently protects against injury at 3 weeks after HI (Northington et al., 2011), it was interesting that Nec-1 delayed PERK phosphorylation beyond 3 hours and in doing so, seemed to prevent full activation of the UPR. Arguably, the metabolic signals sensed as ER stress may differ considerably between the acute 3h time point and the more sub-acute 24 h time point. The significance of the delay and lack of full activation of the UPR after HI with Nec-1 was evidenced by the robust differences in GADD34 expression and XBP-1 transcription and splicing and the mitigation of ER ultrastructural pathology in the forebrain of Nec-1 treated mice. Ultimately, there was no difference in the expression of CHOP at 24 h between vehicle and Nec-1 treated mice. Given the neuroprotection afforded by Nec-1 and the predominance of necrotic forms of cell death in the early time points after HI, it was likely that the small amount of apoptosis resulting from the ~20% increase in CHOP expression was a relatively minor overall contributor to the neuropathology of neonatal HI at acute time points in the neonatal mouse model.

Given the rapidity with which ER stress occurs following HI, immediate therapies to abrogate ER stress are logical. Melatonin significantly reduces the alternative splicing of XBP-1 mRNA, phosphorylation of eIF2α and provides substantial neuroprotection (Carloni et al., 2014b). Both melatonin and Nec-1 achieved significant neuroprotection with significant suppression of ER stress signaling and pathology. However, the studies differ in the effect of each therapy on expression of CHOP, with melatonin effectively blocking CHOP expression in ipsilateral hippocampus and cortex 24 hours after injury (Carloni et al., 2014b), while there was no effect of Nec-1 on CHOP expression in forebrain homogenates 24 hours after injury. Despite general agreement with some differences from the two major papers addressing ER stress in neonatal HI, it appears that the findings observed presently were not strain, or even species specific.

ER morphology is intricately related to its function. The ER is the largest, continuous membrane bound organelle within the cell, and must remain in continuity from the nuclear envelope to association with the plasma membrane (Friedman and Voeltz, 2011). The ER must also maintain a shape that allows other organelles to both be in close proximity (especially mitochondria) and also move freely around the ER within the cytoplasm (Friedman and Voeltz, 2011). Extensive survey of ultrastructural ER morphology following neonatal HI has not been done, but dilated RER at 30 minutes and at 3 hours after HI is documented (Puka-Sundvall et al., 2000). EM studies have shown extensive ER pathology in striatal neurons in a piglet model of neonatal HI (Martin et al., 2000) and in a neonatal rat model of excitotoxicity (Portera-Cailliau et al., 1997). The death of striatal neurons after HI

Author Manuscript Author Manuscript Author Manuscript Author Manuscript

in piglets is categorically necrosis (Martin et al., 2000), contrasting with findings in neonatal rat striatum after HI (Northington et al., 2001). Nevertheless, despite the necrosis, the neurodegeneration in piglets evolves with a specific temporal pattern of subcellular organelle damage and biochemical defects (Martin et al., 2000). Damage to the Golgi apparatus and RER occurs at 3–12 hours, while most mitochondria appear intact until 12 hours (Martin et al., 2000). In contrast, EM shows that during the first 24 hours after excitotoxicity in neonatal rat striatum and cerebral cortex, ER dilatation, Golgi-derived vacuolation, and mitochondrial swelling is successive subcellular changes that then result in neuronal apoptosis. The molecular mechanisms through which similar morphologic changes occurring over a similar temporal framework can result in two distinct forms of neuronal cell death are unclear but these observations provide a basis for the concept of the cell death continuum (Martin, 2001; Martin et al., 1998).

In yeast, when UPR is induced there is proliferation and elongation of ER membrane system, with a 3 fold increase in length and 1.5 fold increase in width (Bernales et al., 2006). This proliferative response may serve to decrease the intraluminal concentration of unfolded proteins thus preventing protein aggregation and allowing more time to fold the proteins properly or degrade them in the face of a stress (Bernales et al., 2006). The huge apparent increases in ER volume in neurons following neonatal HI suggest that if the neurons did not die immediately from catastrophic necrosis, they had an enormous capacity to buffer cell stress by enlargement of the ER compartment. An increased capacity to buffer cell stress is also suggested by the calreticulin immunostaining profile indicative of large increases in calreticulin in stressed neurons within areas of injury. Only at late stages with loss of neuronal structure does calreticulin immunoreactivity abate but then appears to correspondingly increase in reactive glia. The prominent ER enlargement and enhancement of calreticulin immunostaining seen in the present study may also reflect a response to large shifts in Ca^{2+} induced by HI and the need to sequester this Ca^{2+} away from the mitochondria, Ca^{2+} sensitive proteases and other calcium responsive enzymes that would degrade the cell. Deposits of Ca^{2+} in dilated fragments of ER were identified in the original description of ER swelling following neonatal HI (Puka-Sundvall et al., 2000).

Initially the ER dilation is confined to the cytoplasmic tubules followed by blebbing and swelling of ER in continuity with the nuclear envelope. Mild ER dilation without distortion is seen with ischemic preconditioning (IPC) in contrast to severely enlarged and distorted ER found after permanent focal ischemia (Sheng et al., 2012). These and our findings along with the scant changes in nuclear structure with mild and moderate ER dilation are consistent with a hypothesis that initial enlargement of ER seen with EM is a compensatory adaptive response. When ER ultrastructural pathology is fulminant chromatin condensation manifests as overt and irregular chromatin clumps beyond that which appeared as tiny “peppering” of the nucleus. Multiple enzymes responsible for DNA degradation and chromatin packaging require increased levels of intracellular Ca^{2+} (Vosler et al., 2009) to degrade the nuclear contents. The ER may also function directly in DNA degradation and cell death through the SET complex (Fan et al., 2003). In advanced cortical neurodegeneration after HI, nuclear morphology was consistent with a programmed necrosis form of cell death, characterized by nuclear membrane breaks and random clock-face chromatin condensation (Han et al., 2009; Northington et al., 2007).

Author Manuscript Author Manuscript Author Manuscript Author Manuscript

We describe here a novel neuropathology in the context of neonatal HI brain injury. This pathology found in cerebral cortex was associated with degenerating neocortical neurons. It was characterized most prominently by shedding or sloughing of the peripherally located cytoplasm of neuronal cell bodies. These cell fragments were distinct from the cytoplasmic blebs of apoptosis (Martin et al., 1998) because they contained dilated ER vacuoles and cytoplasmic matrix, but apparently did not contain mitochondria or nuclear fragments. These shed fragments containing distended ER were seen in abundance in the neuropil at 96 hours after HI. These shed fragments were not enclosed in the classic double membrane of an autophagosome, and appeared bounded by a residua of the cell membrane. Neurons that appeared to have shed these cytoplasmic fragments were lacking continuity of the cell membrane, additional evidence that these were not ER phagosomes. This process was reminiscent of a larger scale form of zeiosis (Godman et al., 1975) and thus we use the term neuronal macrozeiosis to describe this process in the neonatal mouse brain after HI. A similar form of cell atrophy has been described before with human liver (Pfeifer and Aterman, 1978), rat liver (Yeong et al., 1993), and rat uterus (Henell et al., 1982). That these profound derangements of ER morphology were almost completely lacking in mice treated with Nec-1, suggests that the process leading to these changes was interrupted early after HI. Because autophagy directly counterbalances ER expansion (Bernales et al., 2006) and reduces ER stress after neonatal HI (Carloni et al., 2014a), the shedding of cytoplasmic fragments with ER might be triggered after autophagy survival mechanisms have failed or have been overwhelmed. The proximity of microglia to shed fragments and neurons loosing calreticulin immunoreactivity is evidence of ongoing inflammatory stimulus in these microenvironments, possibly mediated by neuronal macrozeiosis.

As noted, ER morphology is intricately related to its function (Friedman and Voeltz, 2011; Shibata et al., 2010). ER tubules grow along microtubules via sliding dynamics (Friedman and Voeltz, 2011). Microtubule motor protein kinesin-1, which with dynein is integral to ER sliding dynamics, is lost at early stages following neonatal HI (Northington et al., 2007). Whether this loss contributes to ER morphologic abnormalities reported here is unknown. Further investigation of how these ER structural and microtubule motor proteins are affected by HI in the developing brain will be highly relevant to understanding the morphological changes described here.

5. CONCLUSIONS

These findings add strength to the known importance of ER stress in neonatal HI brain pathology. The ultrastructural findings of prominent ER swelling and shedding of cytoplasmic contents containing dilated ER fragments in a macrozeiotic-like process reflect the ability of injured and stressed neonatal neurons to activate survival mechanisms and the prominent role of the ER in determining neuronal cell fate after HI injury. These findings suggest that the ER may be an intracellular biomarker of the severity of injury and the potential for recovery. They also suggest that application of therapies to mitigate progression of ER stress may be applied in a more delayed fashion, with or without other therapies, to rescue stressed neurons with the potential to recover. The protective properties of Nec-1 against this progressive ER pathology and neuronal macrozeiosis warrant further exploration.

Author Manuscript Author Manuscript Author Manuscript Author Manuscript

Acknowledgments

FUNDING SOURCES: FJN is supported by grants HD070996 and HD074593 from the NIH. LJM is supported by grants NS079348 and NS065895 from NIH. RCV is the recipient of Early Career Sutland-Pakula Research Endowment for Neonatal Research. The authors appreciate and acknowledge the expertise of Michael Delanoy for EM preparation and imaging.

ABBREVIATIONS

ATF	activation transcription factor
CHOP	CCAAT/-enhancer-binding protein homologous protein
EIF	eukaryotic initiation factor
EM	electron microscopy
ER	endoplasmic reticulum
GADD	growth arrest and DNA damage-inducible protein
GRP78	78 kd glucose regulated protein (also known as BiP and HSP5a)
HI	hypoxia-ischemia
IQR	interquartile range
IRE	inositol-requiring enzyme
Nec-1	necrostatin-1
p	postnatal day
PERK	protein kinase RNA-like endoplasmic reticulum kinase
UPR	unfolded protein response
XBP	X-box protein

References

Badiola N, et al. Induction of ER stress in response to oxygen-glucose deprivation of cortical cultures involves the activation of the PERK and IRE-1 pathways and of caspase-12. Cell death & disease. 2011; 2

Bernales S, et al. Autophagy counterbalances endoplasmic reticulum expansion during the unfolded protein response. PLoS biology. 2006

Bradford MM. A rapid and sensitive method for the quantitation of microgram quantities of protein utilizing the principle of protein-dye binding. Anal Biochem. 1976; 72:248–54. [PubMed: 942051]

Calfon M, et al. IRE1 couples endoplasmic reticulum load to secretory capacity by processing the XBP-1 mRNA. Nature. 2002; 415:92–6. [PubMed: 11780124]

Carloni S, et al. Increased autophagy reduces endoplasmic reticulum stress after neonatal hypoxia-ischemia: role of protein synthesis and autophagic pathways. Experimental neurology. 2014a; 255:103–112. [PubMed: 24631374]

Carloni S, et al. Melatonin reduces endoplasmic reticulum stress and preserves sirtuin 1 expression in neuronal cells of newborn rats after hypoxia-ischemia. Journal of pineal research. 2014b; 57:192–199. [PubMed: 24980917]

Chalak LF, et al. Biomarkers for severity of neonatal hypoxic-ischemic encephalopathy and outcomes in newborns receiving hypothermia therapy. J Pediatr. 2014; 164:468–74 e1. [PubMed: 24332821]

Author Manuscript Author Manuscript Author Manuscript Author Manuscript

Chavez-Valdez R, et al. Necrostatin-1 attenuates mitochondrial dysfunction in neurons and astrocytes following neonatal hypoxia-ischemia. Neuroscience. 2012a; 219:192–203. [PubMed: 22579794]

Chavez-Valdez R, et al. Programmed Necrosis: A Prominent Mechanism of Cell Death following Neonatal Brain Injury. Neurol Res Int. 2012b; 2012:257563. [PubMed: 22666585]

Ditelberg JS, et al. Brain injury after perinatal hypoxia-ischemia is exacerbated in copper/zinc superoxide dismutase transgenic mice. Pediatr Res. 1996; 39:204–8. [PubMed: 8825788]

Douglas-Escobar M, et al. A pilot study of novel biomarkers in neonates with hypoxic-ischemic encephalopathy. Pediatr Res. 2010; 68:531–6. [PubMed: 20736881]

Fan Z, et al. Tumor suppressor NM23-H1 is a granzyme A-activated DNase during CTL-mediated apoptosis, and the nucleosome assembly protein SET is its inhibitor. Cell. 2003; 112:659–72. [PubMed: 12628186]

Ferriero DM. Neonatal brain injury. N Engl J Med. 2004; 351:1985–95. [PubMed: 15525724]

Friedman JR, Voeltz GK. The ER in 3D: a multifunctional dynamic membrane network. Trends in cell biology. 2011; 21:709–717. [PubMed: 21900009]

Gill MB, Perez-Polo JR. Bax shuttling after rotenone treatment of neuronal primary cultures: effects on cell death phenotypes. J Neurosci Res. 2009; 87:2047–65. [PubMed: 19224578]

Godman GC, et al. Action of cytochalasin D on cells of established lines. III. Zeiosis and movements at the cell surface. The Journal of cell biology. 1975; 64:644–667. [PubMed: 168210]

Gwak M, et al. The effects of dantrolene on hypoxic-ischemic injury in the neonatal rat brain. Anesthesia and analgesia. 2008; 106:227. [PubMed: 18165582]

Han W, et al. Necrostatin-1 reverts shikonin-induced necroptosis to apoptosis. Apoptosis. 2009; 14:674–86. [PubMed: 19288276]

Henell F, et al. An electron microscopic study of the post-partum involution of the rat uterus. Virchows Archiv B. 1982

Hoozemans JJ, et al. The unfolded protein response is activated in Alzheimer's disease. Acta Neuropathol. 2005; 110:165–72. [PubMed: 15973543]

Krishnamoorthy S, Shyam SS. 3-Bromo-7-nitroindazole attenuates brain ischemic injury in diabetic stroke via inhibition of endoplasmic reticulum stress pathway involving CHOP. Life Sciences. 2012; 90:154–160. [PubMed: 22075494]

Markovic SN, Murasko DM. Anesthesia inhibits interferon-induced natural killer cell cytotoxicity via induction of CD8+ suppressor cells. Cell Immunol. 1993; 151:474–80. [PubMed: 8402951]

Martin LJ. Neuronal cell death in nervous system development, disease, and injury (Review). Int J Mol Med. 2001; 7:455–78. [PubMed: 11295106]

Martin LJ, et al. Neurodegeneration in excitotoxicity, global cerebral ischemia, and target deprivation: A perspective on the contributions of apoptosis and necrosis. Brain Res Bull. 1998; 46:281–309. [PubMed: 9671259]

Martin LJ, et al. Neuronal death in newborn striatum after hypoxia-ischemia is necrosis and evolves with oxidative stress. Neurobiol Dis. 2000; 7:169–91. [PubMed: 10860783]

Massaro AN, et al. Serum biomarkers of MRI brain injury in neonatal hypoxic ischemic encephalopathy treated with whole-body hypothermia: a pilot study. Pediatr Crit Care Med. 2013; 14:310–7. [PubMed: 23392373]

Moreno JA, Tiffany-Castiglioni E. The chaperone grp78 in protein folding disorders of the nervous system. Neurochemical research. 2015; 40:329–335. [PubMed: 25107299]

Northington FJ, et al. Necrostatin decreases oxidative damage, inflammation, and injury after neonatal HI. J Cereb Blood Flow Metab. 2011; 31:178–89. [PubMed: 20571523]

Northington FJ, et al. Early Neurodegeneration after Hypoxia-Ischemia in Neonatal Rat Is Necrosis while Delayed Neuronal Death Is Apoptosis. Neurobiol Dis. 2001; 8:207–19. [PubMed: 11300718]

Northington FJ, et al. Nitric oxide synthase 1 and nitric oxide synthase 3 protein expression is regionally and temporally regulated in fetal brain. Dev Brain Res. 1996; 95:1–14. [PubMed: 8873971]

Author Manuscript Author Manuscript Author Manuscript Author Manuscript

Northington FJ, et al. Failure to complete apoptosis following neonatal hypoxia-ischemia manifests as “continuum” phenotype of cell death and occurs with multiple manifestations of mitochondrial dysfunction in rodent forebrain. Neuroscience. 2007; 149:822–33. [PubMed: 17961929]

Paschen W. Endoplasmic reticulum: a primary target in various acute disorders and degenerative diseases of the brain. Cell calcium. 34:365–383. [PubMed: 12909082]

Paschen W, Mengesdorf T. Endoplasmic reticulum stress response and neurodegeneration. Cell calcium. 38:409–415. [PubMed: 16087231]

Pfaffl MW. A new mathematical model for relative quantification in real-time RT-PCR. Nucleic Acids Res. 2001; 29:e45. [PubMed: 11328886]

Pfaffl MW, et al. Determination of stable housekeeping genes, differentially regulated target genes and sample integrity: BestKeeper--Excel-based tool using pair-wise correlations. Biotechnol Lett. 2004; 26:509–15. [PubMed: 15127793]

Pfeifer U, Aterman K. Shedding of peripheral cytoplasm-a mechanism of liver cell atrophy in human amyloidosis. Virchows Archiv B. 1978

Placido AI, et al. Modulation of endoplasmic reticulum stress: an opportunity to prevent neurodegeneration? CNS & neurological disorders drug targets. 2015

Portera-Cailliau C, et al. Excitotoxic neuronal death in the immature brain is an apoptosis-necrosis morphological continuum. The Journal of comparative neurology. 1997; 378:70–87. [PubMed: 9120055]

Puka-Sundvall M, et al. Subcellular distribution of calcium and ultrastructural changes after cerebral hypoxia-ischemia in immature rats. Brain research. Developmental brain research. 2000; 125:31–41. [PubMed: 11154758]

Radford H, et al. PERK inhibition prevents tau-mediated neurodegeneration in a mouse model of frontotemporal dementia. Acta Neuropathol. 2015

Sheng R, et al. Autophagy regulates endoplasmic reticulum stress in ischemic preconditioning. Autophagy. 2012

Shibata Y, et al. Mechanisms determining the morphology of the peripheral ER. Cell. 2010; 143:774–788. [PubMed: 21111237]

Sun X, et al. Development-dependent regulation of molecular chaperones after hypoxia-ischemia. Neurobiol Dis. 2015; 82:123–131. [PubMed: 26070787]

Szegezdi E, et al. Mediators of endoplasmic reticulum stress-induced apoptosis. EMBO Rep. 2006; 7:880–5. [PubMed: 16953201]

Tasker RC, et al. Early postischemic dantrolene-induced amelioration of poly(ADP-ribose) polymerase-related bioenergetic failure in neonatal rat brain slices. J Cereb Blood Flow Metab. 1998; 18:1346–56. [PubMed: 9850147]

Vosler PS, et al. Calcium dysregulation induces apoptosis-inducing factor release: cross-talk between PARP-1- and calpain-signaling pathways. Experimental neurology. 2009; 218:213–220. [PubMed: 19427306]

Wang KK. Calpain and caspase: can you tell the difference?, by kevin K.W. Wang Vol. 23, pp. 20–26. Trends Neurosci. 2000; 23:59. [PubMed: 10652545]

Yeong ML, et al. Hepatocyte membrane injury and bleb formation following low dose comfrey toxicity in rats. Int J Exp Pathol. 1993; 74:211–7. [PubMed: 8499322]

Yoshida H, et al. XBP1 mRNA is induced by ATF6 and spliced by IRE1 in response to ER stress to produce a highly active transcription factor. Cell. 2001; 107:881–91. [PubMed: 11779464]

Yoshida H, et al. ATF6 activated by proteolysis binds in the presence of NF-Y (CBF) directly to the cis-acting element responsible for the mammalian unfolded protein response. Mol Cell Biol. 2000; 20:6755–67. [PubMed: 10958673]

Yuan Y, et al. Ischemic postconditioning protects brain from ischemia/reperfusion injury by attenuating endoplasmic reticulum stress-induced apoptosis through PI3K-Akt pathway. Brain research. 2011; 1367:85–93. [PubMed: 20940001]

Zhu Q-LL, et al. Neuroprotective effects of oxysophocarpine on neonatal rat primary cultured hippocampal neurons injured by oxygen-glucose deprivation and reperfusion. Pharmaceutical biology. 2014; 52:1052–1059. [PubMed: 24601951]

Author Manuscript Author Manuscript Author Manuscript Author Manuscript

HIGHLIGHTS

- Biochemical markers of ER stress precede disruption in ER morphology after HI.
- HI induces progressive ER dilation to maintain homeostasis as mitochondria swell.
- When ER fails, nuclear pathology proceeds toward a form of programmed necrosis.
- In areas of severe HI injury, calreticulin expression within the ER dissipates.
- Necrostatin blocks biochemical ER stress and microstructural ER disruption after HI.

Author Manuscript Author Manuscript Author Manuscript Author Manuscript

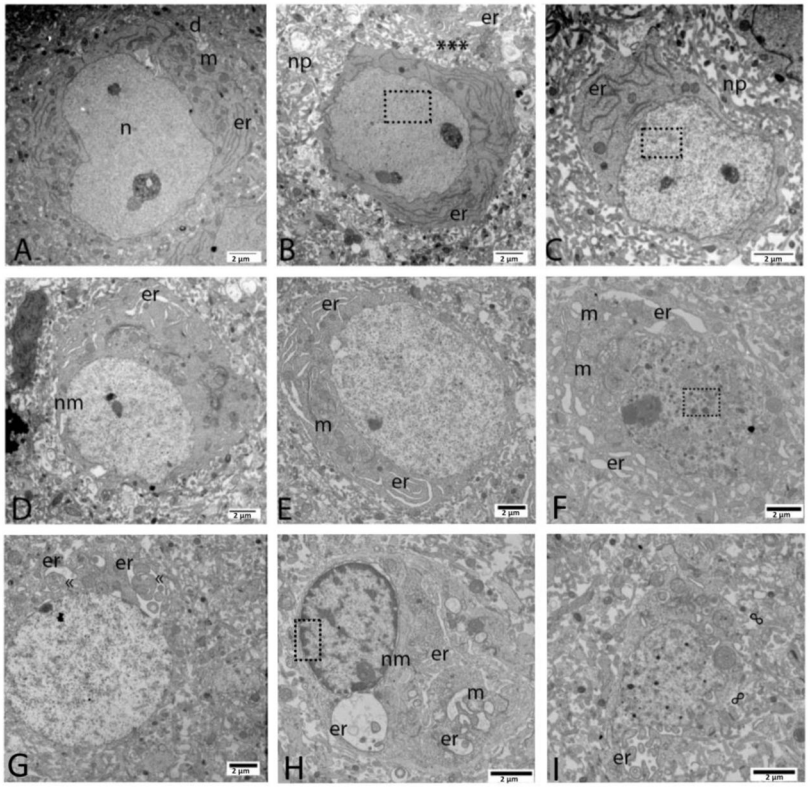

Figure 1.

Representative endoplasmic reticulum (ER) pathology following neonatal HI (n=4 pups). **(A)** Neuron with normal appearing ER (er), mitochondria (m) and nuclear structure (n) were present in neuropil with evidence of very mild dendritic swelling (d). **(B)** Elongation and marginalization of ER (er) was found in a neuron with one darkened mitochondria and very minimal chromatin condensation appearing as a slight peppering of the nucleus (boxed area). Surrounding neuropil (np) was significantly disrupted with a shed cytoplasmic fragment (asterisks) containing much more dilated ER (er) at the top edge of the photomicrograph. **(C)** The earliest signs of swelling were appreciated in elongated and marginalized ER (er) in a neuron with progressive random condensation of nuclear chromatin (boxed area). Surrounding neuropil (np) was significantly disrupted. **(D)** Dilation of ER (er) along the nuclear membrane (nm) was present. **(E)** Dilation throughout the full complement of cytoplasmic ER (er) occurred with swollen appearing mitochondria (m) and still random small condensations of nuclear chromatin. **(F)** Advancement to larger random chromatin fragments (boxed area) was encountered with advanced ER (er) dilation and mitochondrial (m) swelling and disruption. **(G)** Progressive stages of massive ER swelling (er) with pseudo-inclusions («) were encountered within neurons with a similar degree of chromatin breakdown. **(H)** A neuron with complete detachment of the ER from nuclear membrane (nm) including a large bleb, more advanced, “clock-face” nuclear chromatin condensation (boxed area) appeared to be shedding a large fragment of cytoplasm with hugely dilated ER (er) and completely disrupted mitochondria (m) included. **(I)** Neurons with very small amounts of remaining cytoplasm, loss of continuity of the cellular membrane (∞) and advanced pathology of ER (er) may had already shed portions of their

cytoplasmic contents including swollen ER into the neuropil. Larger but still random chromatin condensation occurred in the nucleus. Magnification noted with measure bar in right lower corner of each panel.

Author Manuscript Author Manuscript Author Manuscript Author Manuscript

Author Manuscript Author Manuscript Author Manuscript Author Manuscript

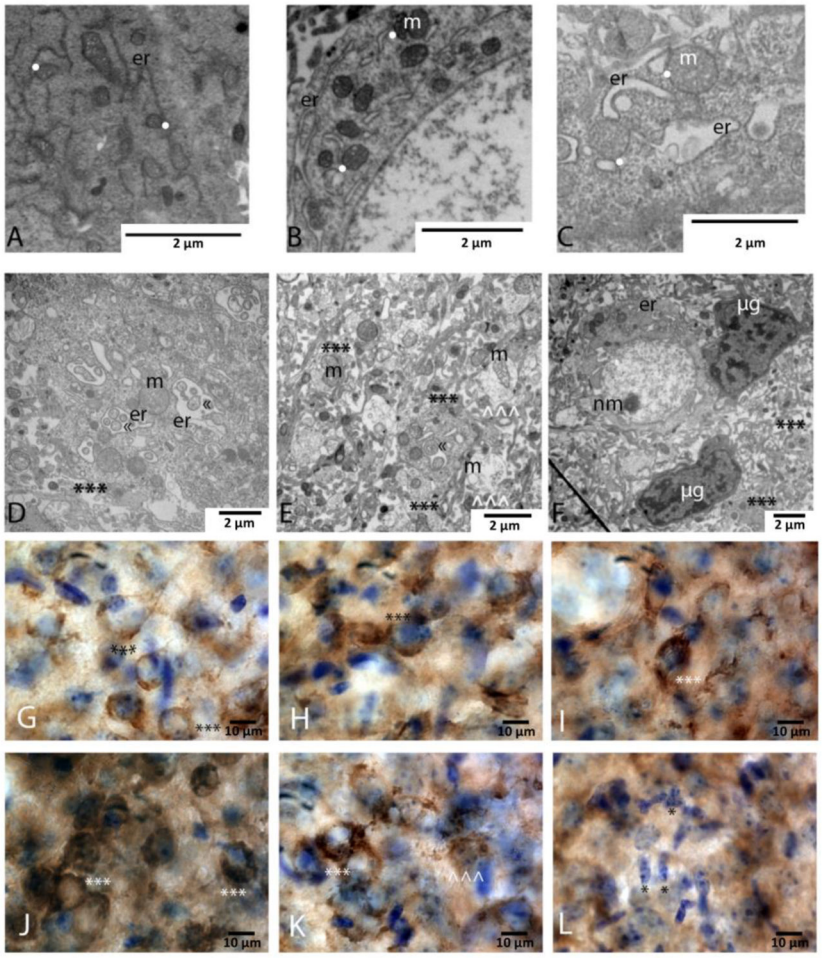

Figure 2.

High resolution and close approximation of endoplasmic reticulum ER fragments with mitochondria within cytoplasmic compartment of neurons following neonatal HI (panels **A–C**). (n=4 pups). **(A)** Minimal ER (er) dilation. **(B)** Progression of ER (er) dilation and multiple contact points (white dots) with mitochondria (m). **(C)** Massively dilated ER (er) encircling clumps of cytoplasm. These massively dilated sections of ER (er) are still found abutting (white dots) swollen mitochondria (m). **(D** and **E)** Representative examples of shed cytoplasmic fragments (***) containing swollen ER (er) with pseudo-inclusions of cytoplasm («). These shed fragments also included large and swollen mitochondria (m). Smaller shed fragments with the same contents as in D (*** in E) within a highly disrupted neuropil containing swollen dendrites (^^^) with swollen and disrupted mitochondria (m). **(F)** Microglia (µg) were attracted to the area of neurons and shed cytoplasmic fragments (***). Neuron and shed cytoplasmic fragments had marked ER (er) pathology including blebbing from the nuclear membrane (nm) in neurons and swelling. Magnification noted with measure bar in right lower corner of each panel. **(G–L)** Calreticulin immunostaining as a marker of ER pathology after neonatal HI. Calreticulin staining in neurons mimicked some of the ultrastructural pathology seen following neonatal HI. **(G)** Healthy pyramidal neurons within layer IV of the cortex display fine, reticular pattern of calreticulin staining (***) at

Author Manuscript Author Manuscript Author Manuscript Author Manuscript

p11. **(H)** Neurons in areas with mild HI injury had increased calreticulin staining in pyramidal neurons (***). **(I and J)** In areas with more advanced injury, increasing numbers of neurons display massive accumulation of calreticulin within the cytoplasm (***). **(K)** In areas with the most severe injury, some neurons had massive accumulation of calreticulin within the cytoplasm, including punctate areas of immunoreactivity suggesting especially high concentrations (***). Other neurons within those areas had lost staining for calreticulin and appeared to be shedding fragments that were still weakly immunoreative for calreticulin (^^^). **(L)** At most advanced stages of injury, minimal calreticulin staining was identified within pyramidal neurons, and large numbers of microglia occupy most of the field (*). Magnification noted with measure bar in right lower corner of each panel.

Author Manuscript Author Manuscript Author Manuscript Author Manuscript

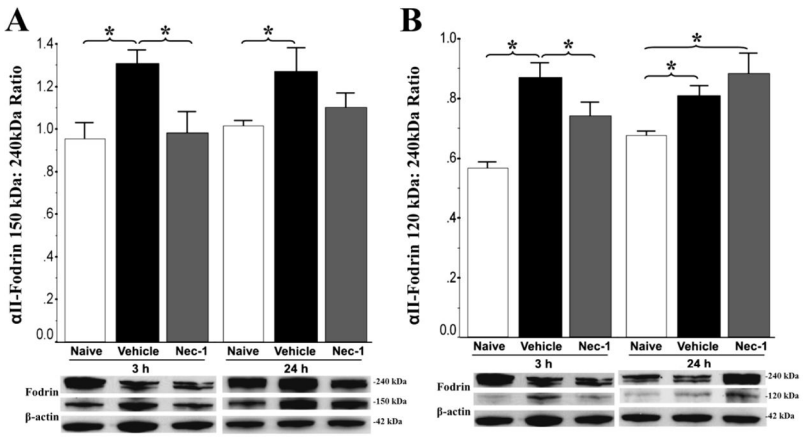

Figure 3.

Early αII-fodrin cleavage as a marker of injury and neuroprotection with necrostatin-1 (Nec-1) treatment in experimental neonatal HI. Bar graphs showing relative cleavage of αII-fodrin (240 kDa) protein into calpain-dependent (150 kDa, **A)** and caspase-dependent (120 kDa, **B)** fragments. Bars represent the mean ± SEM (adjusted OD) measured in forebrain of naive control (white), vehicle (black), and necrostatin (grey) treated male mice. Analysis by one-way ANOVA. *, $p < 0.05$ (Tukey's post-hoc); n= 4 mice/treatment/time. Representative immunoblots with corresponding loading controls (β-actin, 42 kDa) are shown at 3 and 24h.

Author Manuscript Author Manuscript Author Manuscript Author Manuscript

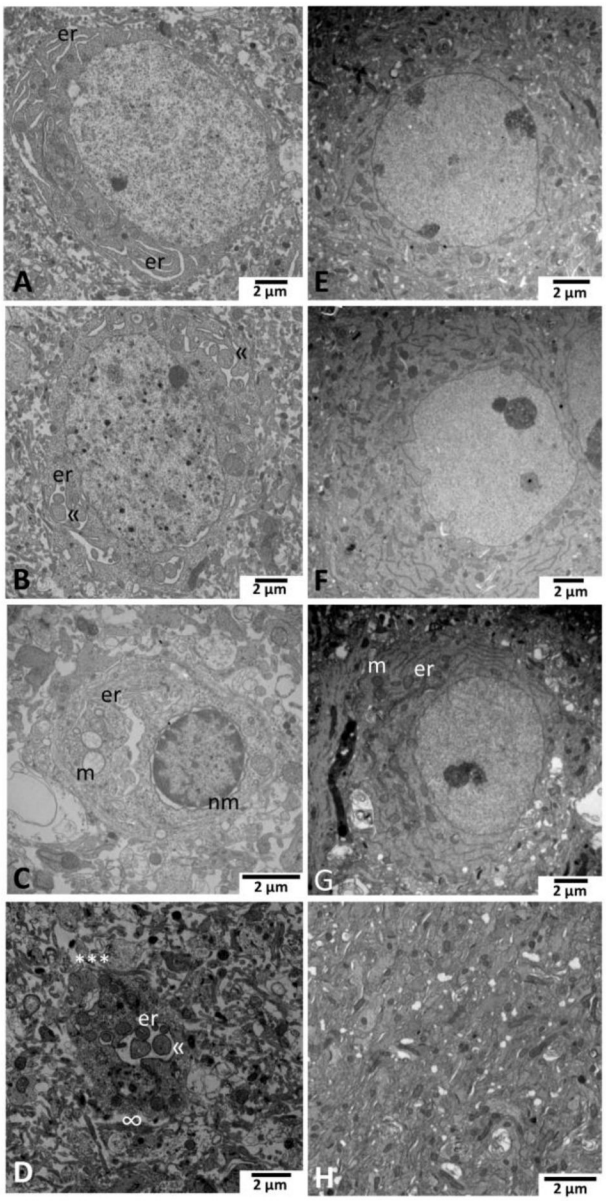

Figure 4.

Necrostatin-1 (Nec-1) protects against endoplasmic reticulum (ER) pathology after neonatal HI (n=4 pups/treatment). Neurons in the ipsilateral cortex at 96 hours after neonatal HI and vehicle treatment (panels **A–D**) display progressive stages of ER dilation and disintegration. **(A)** ER(er) were mildly dilated throughout the cell soma initially, then **(B)** in the moderate stage, more significantly enlarged showing pseudo-inclusions («) of cytoplasm as dilation progresses with mitochondrial swelling and nuclear chromatin randomly condensed. **(C)** Severe ER swelling including that in continuity with the nuclear membrane (nm), accompanies severely swollen and disrupted mitochondria (m) and more, but still random and incomplete chromatin condensation especially around the nuclear margin. **(D)** Shed pieces of neuronal cytoplasm (***) containing swollen ER (er) with the pseudo-inclusions («) of cytoplasm are frequently found in the disrupted neuropil in the cortex of vehicle

Author Manuscript Author Manuscript Author Manuscript Author Manuscript

treated HI injured mice. Not the apparent lack of cell membrane around the shed fragment of cytoplasm (∞). Prominent neuroprotection after neonatal HI and Nec-1 treatment occurs with preservation of ER ultrastructure **(E–H). (E)** Normal appearing neuron with intact ER and mitochondria exists within slightly rarefied neuropil. **(F)** Abundant, intact ER are somewhat marginalized in an otherwise appearing neuron. **(G)** Mild dilation of ER (er) in the cell soma periphery occurs in a neuron with some darkened and rounded mitochondria (m). **(H)** Neuropil in cortex after HI and Nec-1 treatment is largely intact without evidence of shed fragments of cytoplasm containing dilated ER. Magnification noted with measure bar in right lower corner of each panel.

Author Manuscript Author Manuscript Author Manuscript Author Manuscript

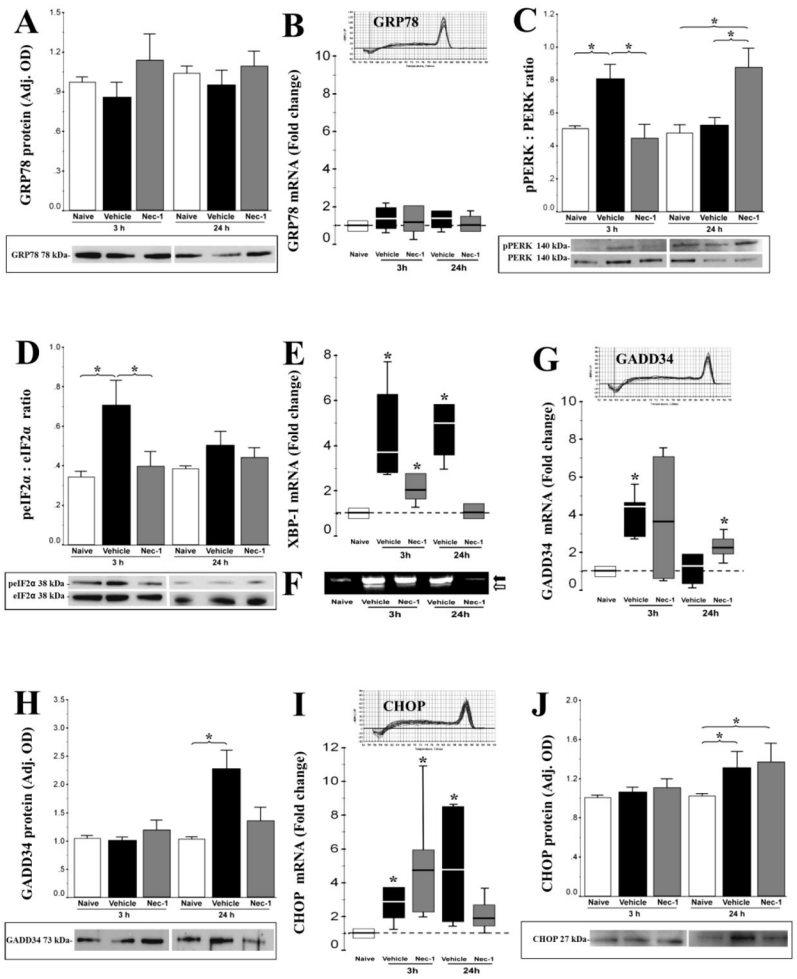

Figure 5.

Endoplasmic reticulum (ER) unfolded protein response (UPR) signaling intermediates at 3 and 24 hours following experimental HI in mice treated with vehicle (black) or necrostatin-1 (Nec-1, grey) vs. naive control (white). ER stress regulator, GRP78 protein **(A)** and mRNA **(B)** levels; phosphorylation of ER sensor PERK **(C)** and downstream eIF2α **(D)** relative to total PERK or eIF2α, respectively; expression of XBP-1 mRNA **(E)** and its unconventional spliced product **(F)** downstream to eIF2α, as well as the negative feedback effector, GADD34 mRNA **(G)** and protein **(H)** are shown. CHOP is a final arbiter of apoptotic cell death in response to ER stress and its changes in mRNA **(I)** and protein **(J)** levels are also shown. Normally distributed data are shown as bar graphs representing mean ± SEM and analyzed one-way ANOVA, while not normally distributed data are shown as box and whiskers plot and analyzed using Mann-Whitney U test (vs. naive control set at 1). Boxes in box and whiskers plots represent the interquartile range (IQR) between 25 to 75 percentiles, the solid line within the box represents the median, and the whiskers extends to the last data point within 1.5 times the IQR. Protein levels were measured by western blot, while mRNA levels were measured by real time qRT-PCR. Figures present data obtained from forebrain homogenates of naive control (white), vehicle (black), and necrostatin (grey) treated mice. *,

Author Manuscript Author Manuscript Author Manuscript Author Manuscript

$p < 0.05$; n= 4 mice/treatment/time per technique. Representative immunoblots **(A, C, D, H, J)** and melting curves **(B, G, I)** are shown.

Author Manuscript Author Manuscript Author Manuscript Author Manuscript

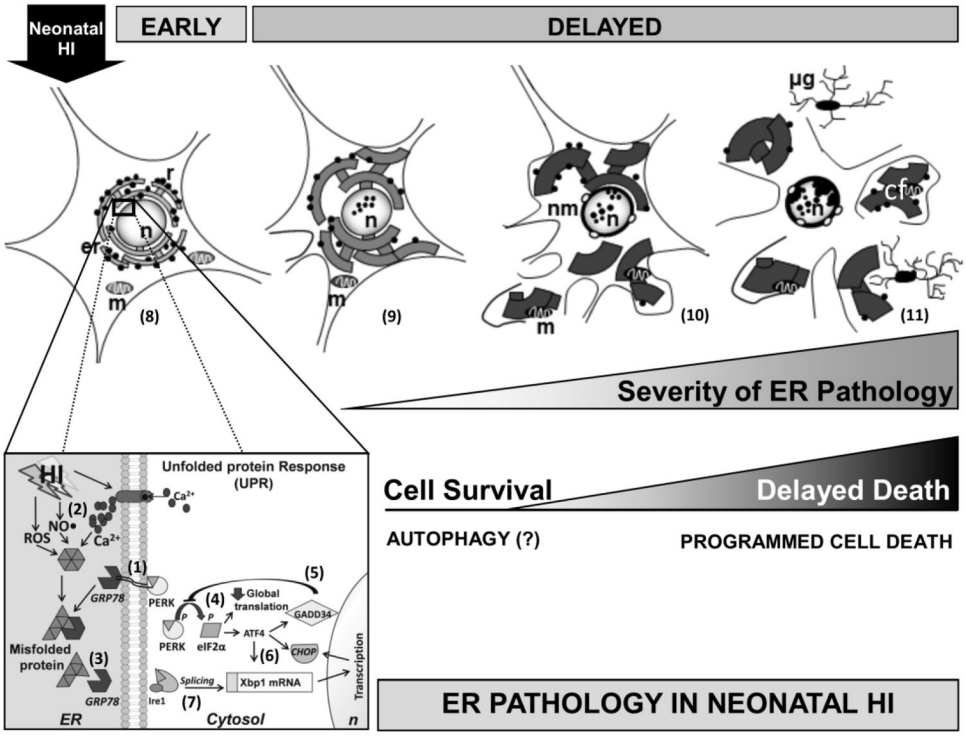

Figure 6.

Simplified schematic representation of the early biochemical markers of ER stress and delayed ER ultrastructural pathology in neurons following neonatal HI. At baseline GRP78, a Ca^{2+} dependent master cell stress regulator found in the ER lumen, binds to ER sensors (PERK, Ire1 and ATF6) **(1)**. Following neonatal HI, reperfusion induces free radical production (ROS, NO•) and Ca^{2+} dysregulation **(2)** and consequently misfolded, damaged, or truncated proteins accumulate and bind to GRP78, releasing PERK and other ER stress sensors **(3)**. These steps initiate the unfolded protein response (UPR) that follows ER stress. After release, PERK oligomerizes, autophosphorylates and induces early phosphorylation of eIF2α producing global translation inhibition with preferential translation of ATF4 **(4)**. ATF4 facilitates GADD34 transcription, which provides negative feedback to limit eIF2α phosphorylation **(5)**, and via Xbox protein (Xbp) 1, increases CHOP transcription **(6)**. Ire1 endonuclease activity also produces splicing of Xbp1mRNA allowing translation of an active protein that becomes part of the transcription complex for CHOP **(7)**. The characterization of individual selectively vulnerable cortical neurons at delayed stages after HI in the mouse permitted the reconstruction of a possible evolution of ER stress related neurodegeneration. Schematic morphology of a cortical neuron showing the rough ER **(er)** bound to ribosomes **(r)** surrounding the nucleus **(n)** and with intact mitochondria **(m) (8).** Mild ER pathology is characterized by distended vermiform ER strands sometimes marginated to the periphery of the cortical neuron and associated in some instances with dark appearing nuclear speckles (peppering) **(9).** Moderate ER pathology includes the formation of large swollen ER cisterns. As ER pathology advances, these fragments of cytoplasm containing dilated ER and in some instances including disrupted mitochondria **(m)** appear to be shed from the neuron in a macrozeiotic-like process. The nucleus may

Author Manuscript Author Manuscript Author Manuscript Author Manuscript

show larger speckles with thickening and blebbling of the nuclear envelope **(10)**. The most severe ER pathology includes significant shedding of hugely dilated ER cisterns within cytoplasmic fragments **(cf)**, along with neuronal volume shrinkage and microglia **(μg)** infiltration **(11)**. While ER stress response with UPR is initiated quickly following neonatal HI, a delayed cell death proceeds with significant intracellular ER pathology proceeds via a form of programmed cell necrosis once ER compensatory and autophagy mechanisms are overwhelmed.

Author Manuscript

Author Manuscript

Author Manuscript

Author Manuscript

TABLE 1

Gene		Sequence	bp	Reference/UniSTS
GRP78	S	5′-TTGCTCACGTGTCTTGGG-3′	159	119720
	AS	5′-TGGTGTCACTTATGGTAGAAAAAAG-3′		
GADD34	S	5′-GTCCATTTCCTTGCTGTCTG-3′		(Badiola et al., 2011)
	AS	5′-AAGGCGTGT-CCATGCTCTGG-3′		
XBP1	S	5′-AAACAGAGTAGCAGCGCAGACTGC-3′	600	(Calfon et al., 2002)
	AS	5′-GGATCTCTAAAACTAGAGGCTTGGTG-3′		
CHOP	S	5′-ACCTCCTGTCTGTCTCTCCG-3′	111	160053
	AS	5′-TCCTGGTCTACCCTCAGTCC-3′		

AS, antisense; **bp,** base-pair; **S,** sense.